Characterization of the Finline Step Discontinuity on Anisotropic Substrates

HUNG-YU YANG, STUDENT MEMBER, IEEE, AND NICÓLAOS G. ALEXÓPOULOS, FELLOW, IEEE

Abstract — **An analysis of the finline step discontinuity in either uniaxial or biaxial substrates is presented. The method is based on a spectral-domain hybrid-mode expansion in an enclosed finline cavity in conjunction with Galerkin's method. A numerically stable scattering matrix formulation is used. The effect of substrate anisotropy is described. The results are also compared with published experimental data or those by the modal matching method when the substrate is isotropic. The comparison shows very good agreement.**

I. INTRODUCTION

FINLINES ARE widely used as millimeter-wave components, and a variety of finline passive and active devices has been realized. The finline step discontinuity has been used as an impedance transformer in MMIC. Anisotropy is present in a variety of practical substrates [1]. It has been shown, for example in [1] and [2], that neglecting substrate anisotropy leads to serious errors in the dispersion characteristics of MIC's or MMIC's. Therefore, it is of practical interest to study the effects of substrate anisotropy on the properties of MIC and MMIC junction discontinuities. Theoretical investigations of finline step discontinuities by modal analysis have been reported by a number of authors [3]–[6] and a transverse resonance method based on the impedance matrix formulation was reported in [7]. Jansen [8] proposed a generalized algorithm for the analysis of planar MIC and MMIC with a spectral-domain approach. Using this approach, certain results on the modeling of junction discontinuities have been reported [8]–[15]. However, no attempt has been made to use this method for the characterization of finline step discontinuities. In fact, the formulation of the boundary value problem in Jansen's spectral-domain method and the transverse resonance technique proposed in [7] are identical. However, in the spectral-domain approach, the goal is to find the incident and reflected wave strength in each port to construct the scattering matrix, while the transverse resonance method [7] aims to find the resonant length of the cavity. Based on the resonant length, the impedance parameters are computed from the resonance condition. Therefore, these two methods are basically the same in theory but they are different in a computer-aided design point of view. The aim of this paper is to generalize the spectral-domain technique such that the substrate anisotropy can be incorporated into the design of finline junction discontinuities in integrated circuits. Although only the finline step discontinuity will be considered here, the modification to other discontinuities should be straightforward.

One of the main features of the spectral-domain method is that two fictitious metallic walls are placed away from the step discontinuity. This allows a complete hybrid-mode expansion inside the cavity except at the interface region where the discontinuity occurs (see Figs. 1 and 2). The hybrid modes in the isotropic region are the superposition of LSE and LSM modes, while the hybrid modes in the biaxial material may be constructed from two coupled-wave equations of the type described in [2] and [16]. In the standard numerical analysis, the unknown electric fields in the aperture region are expanded in terms of a set of known functions. If the basis functions are also transformed into the 2-D Fourier domain, only a one-dimensional boundary value problem needs to be solved. After the Galerkin method is performed, the complete electromagnetic fields inside the cavity can be determined from the solution of a characteristic equation. The dominant-mode incident and reflected waves can then be extracted from the 3-D electromagnetic fields. If the above procedures are performed twice, the scattering parameters of the step discontinuity can be determined. The difference between the current analysis and Jansen's spectral-domain approach is that in this analysis the complete eigenmodes are used as expansion modes in the slot. Thus, besides the wave amplitudes of the incident and reflected waves, the finline characteristics can also be extracted from the 3-D electromagnetic fields.

Since in the above formulation the scattering parameters are directly related to the power flow in the finline, the results are quite stable. The accuracy of this procedure is confirmed by excellent agreement with published experimental data and modal analysis. In contrast, the amplitude of the scattering parameters in [7] differs noticeably from that of modal analysis. The results with sapphire substrate in which the optical axis has various orientations and with the substrate of PTFE cloth ($\epsilon_{xx} = 2.45$, $\epsilon_{yy} = 2.89$, $\epsilon_{zz} = 2.95$) are presented to illustrate the effects of substrate anisotropy.

Manuscript received April 16, 1987; revised July 16, 1987. This work was supported by Research Contracts NSF ECS 82 15409 and MICRO/TRW 85-129.

The authors are with the Electrical Engineering Department, University of California, Los Angeles, CA 90024.

IEEE Log Number 8716913.

0018-9480/87/1100-0956$01.00 ©1987 IEEE

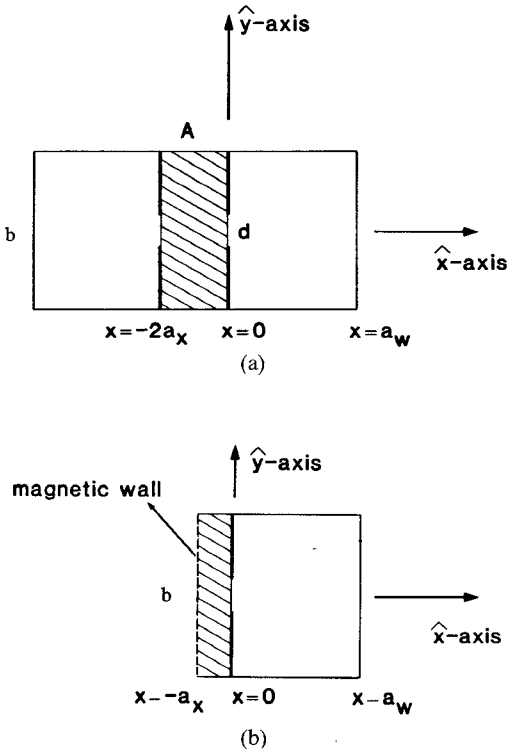

Fig. 1. (a) Cross section of the finline in waveguide. (b) Reduced geometry of Fig. 1(a).

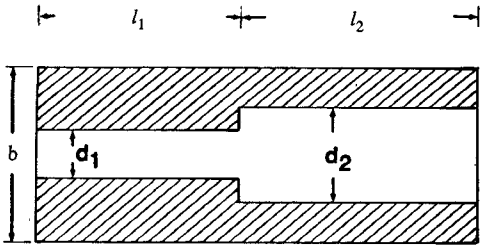

Fig. 2. Finline with a symmetric step discontinuity. $l = l_1 + l_2$.

II. Analytical Formulation

A. Formulation of the Characteristic Equation

Although the method adopted here can be applied to unilateral or antipodal finline, the problem is formulated for bilateral finline only. However, certain results for unilateral finline will be given to provide a comparison with other approaches. The substrate material is assumed to be uniaxial or biaxial and it is described by a permittivity tensor of the form

$$\bar{\bar{\epsilon}} = \epsilon_0 \begin{bmatrix} \epsilon_{xx} & 0 & 0 \\ 0 & \epsilon_{yy} & 0 \\ 0 & 0 & \epsilon_{zz} \end{bmatrix}. \tag{1}$$

The electromagnetic fields in this type of material cannot in general be decomposed into LSE and LSM modes. The wave equations are the coupled partial differential equations given by [2] and [16]:

$$\frac{\epsilon_{yy}}{\epsilon_{xx}}\frac{\partial^2 E_y}{\partial y^2} + \frac{\partial^2 E_y}{\partial x^2} + \frac{\partial^2 E_y}{\partial z^2} - \left(1 - \frac{\epsilon_{zz}}{\epsilon_{xx}}\right)\frac{\partial^2 E_z}{\partial y \partial z} + k_0^2 \epsilon_{yy} E_y = 0 \tag{2}$$

$$\frac{\epsilon_{zz}}{\epsilon_{xx}}\frac{\partial^2 E_z}{\partial z^2} + \frac{\partial^2 E_z}{\partial x^2} + \frac{\partial^2 E_z}{\partial y^2} - \left(1 - \frac{\epsilon_{yy}}{\epsilon_{xx}}\right)\frac{\partial^2 E_y}{\partial y \partial z} + k_0^2 \epsilon_{zz} E_z = 0 \tag{3}$$

and

$$\epsilon_{xx}\frac{\partial E_x}{\partial x} + \epsilon_{yy}\frac{\partial E_y}{\partial y} + \epsilon_{zz}\frac{\partial E_z}{\partial z} = 0. \tag{4}$$

The finline is usually excited by the dominant TE_{10} mode of an empty waveguide. Therefore, because of symmetry, a magnetic wall can be put at $x = -a_x$; thus only the half-structure shown in Fig. 1(b) need be considered. The spectral-domain approach is applied here to a cavity formed by putting two metallic walls away from the discontinuity (Fig. 2). The position of the metallic walls should be chosen such that higher order modes have died out before reaching them. In this manner, transmission line theory can be applied. The spectral-domain method allows one to transform the EM fields inside the cavity into the two-dimensional (y and z) spectral domains, thus reducing the task to the solution of a one-dimensional boundary value problem. The transverse fields with respect to the x axis in the air region can be expanded in terms of LSE and LSM modes, while the transverse fields in the anisotropic region are obtained by solving the fourth-order ordinary differential equation resulting from the Fourier transform of (2)–(4) in [2] and [16]. As a result, the transverse E- and H-field components in the two regions are:

Region I — Anisotropic Region, $-a_x \leqslant x \leqslant 0$:

$$E_{y1} = \sum_{n=1}^{\infty} A'_{0n} \cos\beta_{0n}(x + a_x)\Psi_{0n} + \sum_{n=1}^{\infty}\sum_{m=1}^{\infty} [d_1 A'_{mn} \cos\beta_{mn1}(x + a_x) + d_2 B'_{mn} \cos\beta_{mn2}(x + a_x)]\Psi_{mn} \tag{5}$$

$$E_{z1} = \sum_{m=1}^{\infty} B'_{m0} \cos\beta_{m0}(x + a_x)\Phi_{0n} + \sum_{n=1}^{\infty}\sum_{m=1}^{\infty} [A'_{mn} \cos\beta_{mn1}(x + a_x) + B'_{mn} \cos\beta_{mn2}(x + a_x)]\Phi_{mn} \tag{6}$$

$$H_{y1} = \frac{-1}{j\omega\mu_0}\left\{ \sum_{m=1}^{\infty} B'_{m0}\beta_{m0} \sin\beta_{m0}(x + a_x)\Phi_{0n} + \sum_{n=1}^{\infty}\sum_{m=1}^{\infty} [d_5 A'_{mn} \sin\beta_{mn1}(x + a_x) + d_6 B'_{mn} \sin\beta_{mn2}(x + a_x)]\Phi_{mn} \right\} \tag{7}$$

$$H_{z1}=\frac{-1}{j\omega\mu_0}\left\{\sum_{n=1}^{\infty}-A'_{0n}\beta_{0n}\sin\beta_{0n}(x+a_x)\Psi_{0n}+\sum_{n=1}^{\infty}\sum_{m=1}^{\infty}\left[d_3A'_{mn}\sin\beta_{mn1}(x+a_x)+d_4B'_{mn}\sin\beta_{mn2}(x+a_x)\right]\Psi_{mn}\right\}. \tag{8}$$

Region II — Air Region, $0\leqslant x\leqslant a_w$:

$$E_{y2}=\sum_{m=0}^{\infty}\sum_{n=0}^{\infty}\left[\frac{-n\pi}{l}A_{mn}-\frac{1}{j\omega\epsilon_0}\left(\frac{2m\pi}{b}\right)k_{mn}B_{mn}\right]\cdot\sin k_{mn}(x-a_w)\Psi_{mn} \tag{9}$$

$$E_{z2}=\sum_{m=0}^{\infty}\sum_{n=0}^{\infty}\left[\frac{2m\pi}{b}A_{mn}-\frac{1}{j\omega\epsilon_0}\left(\frac{n\pi}{l}\right)k_{mn}B_{mn}\right]\cdot\sin k_{mn}(x-a_w)\Phi_{mn} \tag{10}$$

$$H_{y2}=\sum_{m=0}^{\infty}\sum_{n=0}^{\infty}\left[\frac{1}{j\omega\mu_0}\left(\frac{2m\pi}{b}\right)k_{mn}A_{mn}+\left(\frac{n\pi}{l}\right)B_{mn}\right]\cdot\cos k_{mn}(x-a_w)\Phi_{mn} \tag{11}$$

$$H_{z2}=\sum_{m=0}^{\infty}\sum_{n=0}^{\infty}\left[\frac{1}{j\omega\mu_0}\left(\frac{n\pi}{l}\right)k_{mn}A_{mn}-\left(\frac{2m\pi}{b}\right)B_{mn}\right]\cdot\cos k_{mn}(x-a_w)\Psi_{mn} \tag{12}$$

where

$$a_1=k_0^2\epsilon_{zz}-\left(\frac{2m\pi}{b}\right)^2-\frac{\epsilon_{zz}}{\epsilon_{xx}}\left(\frac{n\pi}{l}\right)^2 \tag{13}$$

$$a_2=\left(1-\frac{\epsilon_{yy}}{\epsilon_{xx}}\right)\left(\frac{2m\pi}{b}\right)\left(\frac{n\pi}{l}\right) \tag{14}$$

$$b_1=k_0^2\epsilon_{yy}-\left(\frac{n\pi}{l}\right)^2-\frac{\epsilon_{yy}}{\epsilon_{xx}}\left(\frac{2m\pi}{b}\right)^2 \tag{15}$$

$$b_2=\left(1-\frac{\epsilon_{zz}}{\epsilon_{xx}}\right)\left(\frac{2m\pi}{b}\right)\left(\frac{n\pi}{l}\right) \tag{16}$$

$$\beta_{mn1}=\sqrt{\frac{(a_1+b_1)+\sqrt{(a_1-b_1)^2+4a_2b_2}}{2}} \tag{17}$$

$$\beta_{mn2}=\sqrt{\frac{(a_1+b_1)-\sqrt{(a_1-b_1)^2+4a_2b_2}}{2}} \tag{18}$$

$$d_1=\frac{\beta_{mn1}^2-a_1}{a_2} \tag{19}$$

$$d_2=\frac{\beta_{mn2}^2-a_1}{a_2} \tag{20}$$

$$d_3=-d_1\beta_{mn1}-\frac{2m\pi}{b\beta_{mn1}}\left(\frac{\epsilon_{yy}}{\epsilon_{xx}}\frac{2m\pi}{b}d_1+\frac{\epsilon_{zz}}{\epsilon_{xx}}\frac{n\pi}{l}\right) \tag{21}$$

$$d_4=-d_2\beta_{mn2}-\frac{2m\pi}{b\beta_{mn2}}\left(\frac{\epsilon_{yy}}{\epsilon_{xx}}\frac{2m\pi}{b}d_2+\frac{\epsilon_{zz}}{\epsilon_{xx}}\frac{n\pi}{l}\right) \tag{22}$$

$$d_5=\beta_{mn1}-\frac{n\pi}{l\beta_{mn1}}\left(\frac{\epsilon_{yy}}{\epsilon_{xx}}\frac{2m\pi}{b}d_1+\frac{\epsilon_{zz}}{\epsilon_{xx}}\frac{n\pi}{l}\right) \tag{23}$$

$$d_6=\beta_{mn2}-\frac{n\pi}{l\beta_{mn2}}\left(\frac{\epsilon_{yy}}{\epsilon_{xx}}\frac{2m\pi}{b}d_2+\frac{\epsilon_{zz}}{\epsilon_{xx}}\frac{n\pi}{l}\right) \tag{24}$$

$$k_{mn}=\sqrt{k_0^2-\left(\frac{2m\pi}{b}\right)^2-\left(\frac{n\pi}{l}\right)^2} \tag{25}$$

$$\Psi_{mn}=\sqrt{\frac{2\delta_n\delta_m}{lb}}\cos\left(\frac{2m\pi}{b}y\right)\sin\left(\frac{n\pi}{l}z\right) \tag{26}$$

$$\Phi_{mn}=\sqrt{\frac{2\delta_n\delta_m}{lb}}\sin\left(\frac{2m\pi}{b}y\right)\cos\left(\frac{n\pi}{l}z\right) \tag{27}$$

and

$$\delta_p=\begin{cases}1, & p=0\\ 2, & p\neq 0.\end{cases} \tag{28}$$

In what follows, the resonant length of the cavity as a function of operating frequency is determined based on Galerkin's method. The electric fields in the aperture region at the interface ($x=0$) are expanded in terms of a set of known functions. In order to provide less brute force and more reliable results, the basis functions are chosen to form a complete set. For the step discontinuity under consideration, a complete set of eigenfunctions can be obtained by the electric fields in the cross section of a stepped waveguide. The discussion of the method to construct the basis functions will be presented later. The electric field components in the aperture region can be written as

$$E_{y0}=\sum_v V_v e_{yv} \tag{29}$$

and

$$E_{z0}=\sum_v V_v e_{zv} \tag{30}$$

where e_{yv} and e_{zv} are the eigenmodes of a stepped waveguide. Applying the boundary conditions at the air–dielectric interface ($x=0$), the unknowns A_{mn}, B_{mn}, A'_{mn}, and B'_{mn} can be eliminated. The results are a system of homogeneous linear equations in terms of the unknown coefficients V_v:

$$[L][V]=0 \tag{31}$$

where

$$
\begin{aligned}
L_{uv} = & \sum_{m=1}^{\infty} \beta_{m0} \tan(\beta_{m0} a_x) \chi_{m0v} \chi_{m0u} \\
& + \sum_{n=1}^{\infty} \beta_{0n} \tan(\beta_{0n} a_x) \xi_{0nv} \xi_{0nu} \\
& + \sum_{m=1}^{\infty} \sum_{n=1}^{\infty} \left[\left(\frac{d_5 \chi_{mnu} - d_3 \xi_{mnu}}{d_1 - d_2} \right) \right. \\
& \cdot \tan(\beta_{mn1} a_x)(\xi_{mnv} - d_2 \chi_{mnv}) \\
& + \left(\frac{d_6 \chi_{mnu} - d_4 \xi_{mnu}}{d_1 - d_2} \right) \\
& \left. \cdot \tan(\beta_{mn2} a_x)(d_1 \chi_{mnv} - \xi_{mnv}) \right] \\
& + \sum_{m=0}^{\infty} \sum_{n=0}^{\infty} \left[k_{mn} \cot(k_{mn} a_w) \right. \\
& \cdot \frac{\left(\frac{n\pi}{l} \xi_{mnv} - \frac{2m\pi}{b} \chi_{mnv} \right)}{\left(\frac{n\pi}{l} \right)^2 + \left(\frac{2m\pi}{b} \right)^2} \left(\frac{2m\pi}{b} \chi_{mnu} - \frac{n\pi}{l} \xi_{mnu} \right) \\
& - \frac{\cot(k_{mn} a_w)}{k_{mn}} k_0^2 \frac{\left(\frac{n\pi}{l} \chi_{mnv} + \frac{2m\pi}{b} \xi_{mnv} \right)}{\left(\frac{n\pi}{l} \right)^2 + \left(\frac{2m\pi}{b} \right)^2} \\
& \left. \cdot \left(\frac{2m\pi}{b} \xi_{mnu} + \frac{n\pi}{l} \chi_{mnu} \right) \right] \qquad (32)
\end{aligned}
$$

$v = 1, 2, 3, \cdots$, $u = 1, 2, 3, \cdots$, and $m = n = 0$ is excluded. Also

$$\xi_{mnv} = \int_{s_0} \Psi_{mn} e_{yv} \, ds \qquad (33)$$

and

$$\chi_{mnv} = \int_{s_0} \Phi_{mn} e_{zv} \, ds. \qquad (34)$$

B. Constructing the Scattering Matrix

Once the characteristic equation is solved, the complete electromagnetic field inside the cavity can be determined. The next step is to use microwave network theory to extract the information of the junction discontinuity from the obtained EM field. As pointed out by Jansen [8], for the two-port network, exactly two fictitious numerical experiments need to be performed. In other words, with reference to Fig. 2, the characteristic equation is solved twice, for a frequency, for two sets of resonant lengths l_1 and l_2. As a result, the incident and reflected wave strengths are related through

$$B_i^{(k)} = -A_i^{(k)} e^{2j\beta_i l_i^{(k)}} \qquad (35)$$

where i and k represent the ith port in the kth numerical experiment and the reference planes are at the step junction. The wave strength (A_i or B_i) is determined by the solution of the characteristic equation. That is, once (31) is solved, the expansion coefficients and aperture electric fields can be determined accordingly. The voltage wave and propagation constant of each port can be obtained from the aperture electric fields through

$$V(z) = \int_{-b/2}^{b/2} E_{y0}(y, z) \, dy. \qquad (36)$$

That is, one can plot out the function $V(z)$ (voltage wave) to find the propagation constant and wave amplitude in each side of the step junction. The propagation constant or guided wavelength is found from the distance between voltage maxima and minima, while from (35) and $V(z)_{\max}$, one is able to determine the A and B matrices. In the above procedure, it is important that the values of l_1 and l_2 be large enough so that the voltage wave and guided wavelength of the dominant mode can be accurately determined from the peak of $V(z)$ in (36). In other words, the condition of $l_i \geq \lambda_i/4$ should be satisfied such that higher order modes die out before reaching the voltage wave maximum. As a result, the scattering matrix can be obtained as

$$\begin{bmatrix} S_{11} & S_{12} \\ S_{21} & S_{22} \end{bmatrix} = \begin{bmatrix} B_1^1 & B_1^2 \\ B_2^1 & B_2^2 \end{bmatrix} \begin{bmatrix} A_1^1 & A_1^2 \\ A_2^1 & A_2^2 \end{bmatrix}^{-1}. \qquad (37)$$

C. Basis Functions of the Finline with a Step Discontinuity

The formulation in the above two sections is quite general and is valid for a class of discontinuities in microwave and millimeter-wave guiding structures. The above generalized algorithm has the feature that for different types of junction discontinuities, the formulation is different only in the choice of basis functions. However, it should be noted that hybrid numerical techniques may be required for a specific type of discontinuities. For the step discontinuity under consideration, the slot patterns are assumed to be symmetric with respect to the waveguide narrow wall. Therefore, one can put an electric wall at $y = 0$. In the numerical procedure, different types of expansion functions are possible. The point matching method is particularly useful for sophisticated discontinuities, for example, the tapered transition. However, the computer cost is usually enormously large. Jansen [8] used a modified mode-matching technique. He used mode expansions only in the vicinity of the junction to take into account the higher order modes and the entire domain standing wave modes obtained from two-dimensional analysis to represent the dominant mode of the specific guiding structure. This has the advantage that the proper edge condition can be taken into account in the expansion functions. Here the complete eigenmode expansions are used, which are similar to those adopted by Sorrentino and Itoh [7]. The

eigenfunctions in stepped waveguide are composed of TE and TM modes.

For TE eigenfunctions, the fields can be derived from a scalar potential $\Psi(y, z)$:

$$E^{(\mathrm{TE})} = -\hat{x} \times (\nabla \Psi) \tag{38}$$

and

$$\Psi = \begin{cases} \sum_{r=0}^{\infty} A_r \Psi_r^{(1)} & \text{in } s_1 \\ \sum_{s=0}^{\infty} B_s \Psi_s^{(2)} & \text{in } s_2 \end{cases} \tag{39}$$

where

$$\Psi_r^{(1)} = \cos k_{1r} z \cos\left(\frac{2r\pi y}{d_1}\right) \tag{40}$$

$$\Psi_s^{(2)} = \cos k_{2s}(z-l) \cos\left(\frac{2s\pi y}{d_2}\right) \tag{41}$$

$$k_{1r} = \sqrt{k_c^2 - \left(\frac{2r\pi}{d_1}\right)^2} \tag{42}$$

and

$$k_{2s} = \sqrt{k_c^2 - \left(\frac{2s\pi}{d_2}\right)^2}. \tag{43}$$

For TM eigenfunctions, the fields can be derived from a scalar potential $\phi(y, z)$:

$$E^{(\mathrm{TM})} = \nabla \phi \tag{44}$$

and

$$\phi = \begin{cases} \sum_{r=1}^{\infty} A_r \phi_r^{(1)} & \text{in } s_1 \\ \sum_{s=1}^{\infty} B_s \phi_s^{(2)} & \text{in } s_2 \end{cases} \tag{45}$$

where

$$\phi_r^{(1)} = \sin k_{1r} z \sin\left(\frac{2r\pi y}{d_1}\right) \tag{46}$$

$$\phi_s^{(2)} = \sin k_{2s}(z-l) \sin\left(\frac{2s\pi y}{d_2}\right). \tag{47}$$

The k_c is the eigenvalue of the boundary value problem of the stepped waveguide. For each k_c, there corresponds an eigenmode or a basis function. The solutions of k_c are determined from the characteristic equations obtained by the boundary condition at the step junction [7], [16].

III. Numerical Analysis

Based on the analytical formulation described in the last section, numerical computations are performed. The accuracy of the numerical results depends on the truncation of the double Fourier series m and n, the number of basis functions (eigenmodes) v, and the transverse expansion terms r and s in each eigenmode. It is found that in each eigenmode, even a few expansion terms (r and s) can provide excellent resolution of the field distribution in a stepped waveguide. Typically, $r = s = 4$ is used. As mentioned in the last section, the eigenmodes that construct the basis functions are composed of both TE and TM modes for a stepped waveguide. It is observed that the TE eigenmodes have a dominant effect on the property of the step junction. This may be due to the fact that in the finline structure the longitudinal electric field in the slot (E_z) is usually much smaller than the tranverse component (E_y). Also, the first few TE eigenmodes contain the information of the E_y component and have no E_z of the finline dominant mode. Therefore, the first few TE eigenmodes can take into account mostly the dominant mode as well as the corresponding evanescent modes. This behavior can be observed from the sign of k_{1r}^2 and k_{2s}^2 in (39) and (40). Therefore, in the numerical analysis, the first four TE eigenmodes and the first two TM eigenmodes are used. This is equivalent to the total of 48 ($6\times4+6\times4$) entire domain modes that are used to expand the electric fields in the aperture. It has been well addressed by many authors, e.g., [17]–[19], that in the mode matching of iris-type discontinuities, relative convergence problems will occur if the edge condition is not taken into account in the expansion functions. Therefore, it has been recommended that the truncation of the Fourier terms be chosen such that the spatial resolution of each highest Fourier term is about the same. For the standard waveguide dimension, the Fourier terms used are typically less than 50. The main computer cost is to find the cavity lengths l_1 and l_2 at an operating frequency. The procedure requires the iteration of the characteristic function in (31), which contains triple summation. Since in each iteration, only the longitudinal dimension is changed, the transverse Fourier terms need to be computed only at the beginning of the iteration. This procedure can greatly reduce the computer cost. The computer time for solving (31) is typically one minute on the IBM 3090 system.

The current analysis is first checked against the experimental results reported in [5]. The measurement was performed with one side of the finline short-circuited ($l_2 = 0.3$ cm) and the reflection coefficient was measured at the other side 1.1 cm from the junction. The Fourier terms are chosen as $m = n = 20$. The comparison is shown in Fig. 3. It is seen that there is very good agreement within the plotting accuracy. The present analysis has the feature that the propagation constants of each finline section are determined from the 3-D electromagnetic fields (described in the last section) instead of precalculated values from the 2-D spectral-domain analysis. This may avoid the possible mismatch when computing scattering parameters. Since the wave amplitudes are obtained from the slot E_y component and the characteristic impedance is not determined yet, the computed scattering matrix is not normalized. One thing is that although the definition of characteristic impedance is quite arbitrary, the impedance ratio of the

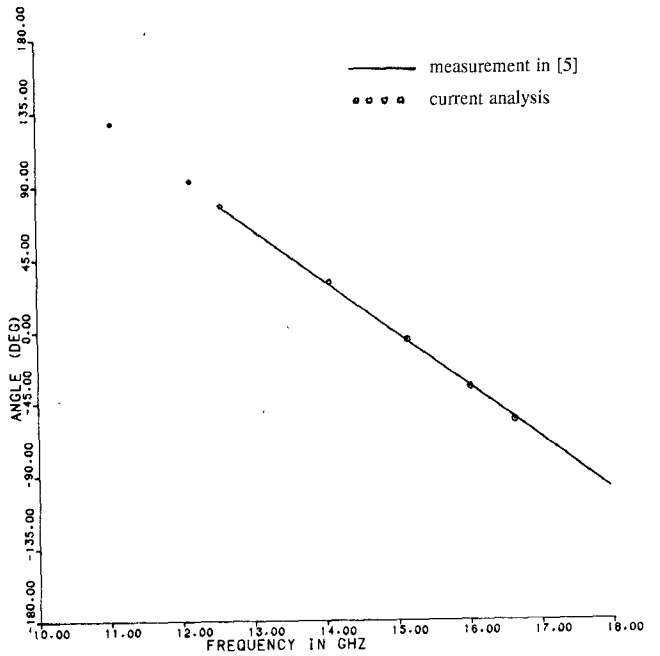

Fig. 3. Phase of the reflection coefficient when port 2 is shorted. WR-62 unilateral finline with $a_x = 0.127$ mm, $\epsilon_r = 2.22$, $d_1 = 0.8$ mm, $d_2 = 4$ mm, $l_2 = 3$ mm, and reference distance = 11 mm.

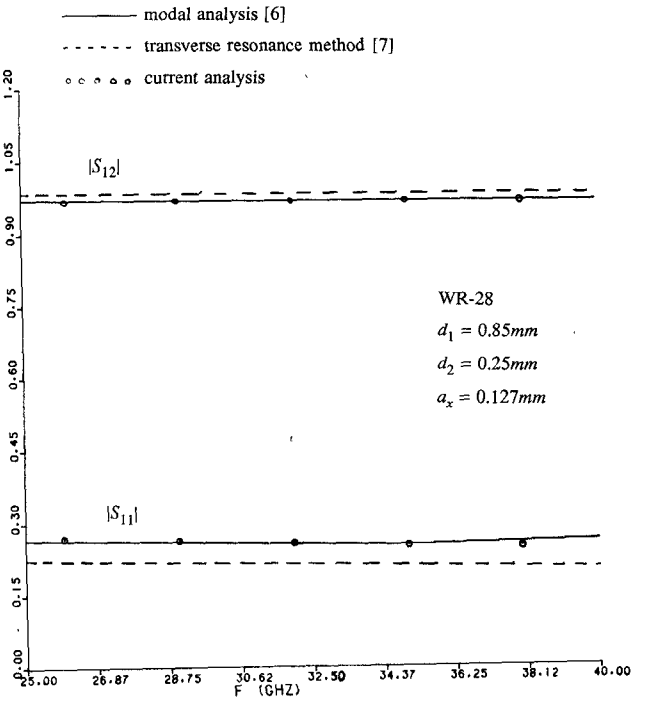

Fig. 4. Magnitude of the scattering parameters of a unilateral finline step discontinuity. $\epsilon_r = 2.22$.

TABLE I

COMPARISON OF 2-D SPECTRAL-DOMAIN ANALYSIS AND EXTRACTED SOLUTIONS FROM 3-D EM FIELDS

f(GHz)	λ_2^a	λ_2^b	λ_1^a	λ_1^b	Z_{02}^a/Z_{01}^a	Z_{02}^b/Z_{01}^b
26	1.403	1.392	1.204	1.200	1.597	1.609
29	1.165	1.156	1.035	1.036	1.555	1.558
32	1.006	0.992	0.913	0.916	1.530	1.528
35	0.889	0.884	0.818	0.820	1.517	1.488
38	0.799	0.788	0.741	0.748	1.510	1.468

WR-28 with $\epsilon_{xx} = 2.45$, $\epsilon_{yy} = 2.89$, $\epsilon_{zz} = 2.95$, $a_x = 0.127$ mm, $d_1 = 1$ mm, and $d_2 = 2$ mm.
(a) 2-D spectral-domain analysis.
(b) Extracted solutions from 3-D EM fields.

TABLE II

COMPARISON OF SAPPHIRE SUBSTRATE WITH DIFFERENTLY ORIENTED OPTICAL AXIS

d_2/d_1	$\|S_{11}\|^a$	$\|S_{11}\|^b$	$\|S_{12}\|^a$	$\|S_{12}\|^b$
1.5	0.144	0.136	0.990	0.991
2.0	0.242	0.235	0.970	0.972
2.5	0.322	0.313	0.947	0.950
3.0	0.395	0.389	0.920	0.921

WR-62, $f = 14$ GHz, $a_x = 0.127$ mm.
(a) $\epsilon_{xx} = \epsilon_{zz} = 9.4$ and $\epsilon_{yy} = 11.6$.
(b) $\epsilon_{yy} = \epsilon_{zz} = 9.4$ and $\epsilon_{xx} = 11.6$.

finline in each side of the step junction should be fixed. From network theory, the unitary property of a normalized scattering matrix allows one to determine the characteristic impedance ratio. In other words, S_{11} or S_{22} is the same regardless of whether the wave amplitude is normalized, and the normalized S_{12} or S_{21} can be deduced from S_{11} and S_{22}. The impedance transform ratio can be obtained from unnormalized S_{12}/S_{21}. The guided wavelength or impedance ratio computed from the 3-D analysis may be compared with those from the 2-D spectral-domain method [2] to confirm the validity of the current analysis. An example of the comparison is shown in Table I. It is seen that the discrepancy is typically less than 1 percent and the agreement is excellent. The reason for this agreement is that once the complete EM fields inside the cavity are determined, these fields contain all the information pertinent to the determination of the equivalent circuit parameters.

It has been shown that the magnitude of the scattering parameters obtained by modal analysis [6] and the transverse resonance method [7] differ noticeably. It is observed that the present analysis is in excellent agreement with modal analysis. A comparison of the three different approaches is shown in Fig. 4. The impedance matrix formulation of the transverse resonance method reported in [7] has the feature that the propagation constants and the characteristic impedance are computed from the 2-D analysis and the power distribution is indirectly related to the

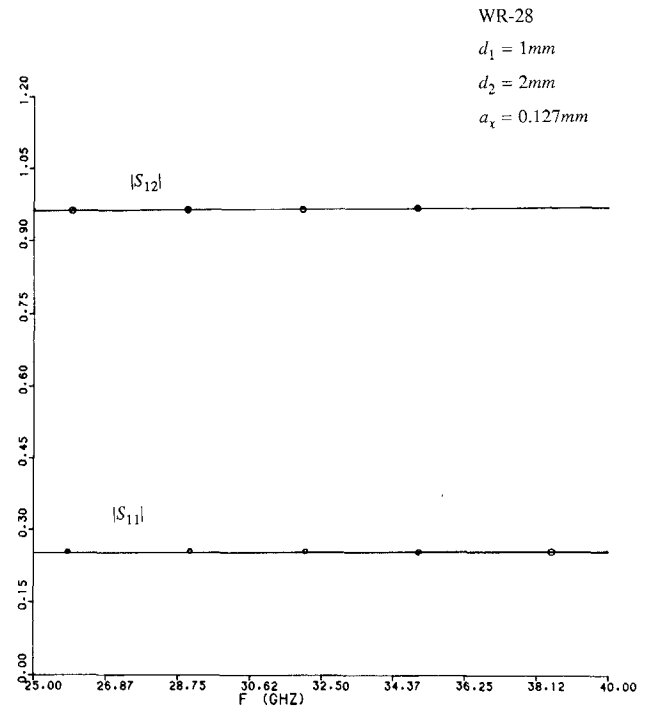

Fig. 5 Magnitude of the scattering parameters. $\epsilon_{xx} = 2.45$, $\epsilon_{yy} = 2.89$, and $\epsilon_{zz} = 2.95$.

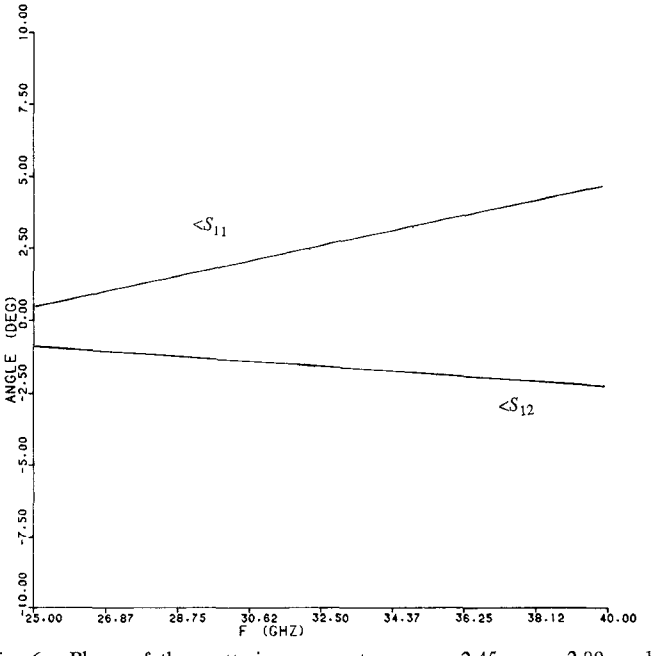

Fig. 6. Phase of the scattering parameters. $\epsilon_{xx} = 2.45$, $\epsilon_{yy} = 2.89$, and $\epsilon_{zz} = 2.95$.

scattering parameters from the numerical computation point of view. In addition, for each scattering matrix computation, three sets of cavity lengths are required instead of two in the present analysis.

The effects of the anisotropic substrate on the properties of the finline step discontinuity are investigated with a sapphire substrate having $\epsilon_t = 9.4$ and $\epsilon_l = 11.6$ as an example. The optical axis is directed in either the $\hat{x}$ or the $\hat{y}$ direction. The computed results are shown in Table II. It is found that the substrate has less effect on the scattering parameters than on the propagation constant. A differently oriented optical axis results typically in a 3–5-percent difference in $|S_{11}|$. The frequency-dependent scattering parameters of the finline step discontinuity on PTFE cloth material ($\epsilon_{xx} = 2.45$, $\epsilon_{yy} = 2.89$, $\epsilon_{zz} = 2.95$) [20] are shown in Figs. 5 and 6. It is observed that the results, especially for the magnitude, are insensitive to frequency change. This is due to the fact that the power reflected $|S_{11}|^2$ and transmitted $|S_{12}|^2$ depends mainly on the impedance transform ratio, which is typically frequency insensitive except near the cutoff frequency. Also, the $|S_{11}|$ is qualitatively proportional to the characteristic impedance ratio.

IV. Conclusions

A modified three-dimensional spectral-domain approach has been applied to characterize the finline step discontinuity on anisotropic substrates. The results are numerically stable and in good agreement with both measurement and modal analysis. The propagation constant of the finline in each section and the characteristic impedance ratio are also obtained from the current three-dimensional hybrid-mode analysis. These results are in good agreement with those computed from two-dimensional full-wave analysis. This comparison also confirms the validity of the current analysis. In contrast, in Jansen's spectral-domain approach, the propagation constant had to be precalculated. The substrate anisotropy is found to have less effect on the network than on the dispersion parameters. The present approach may be modified to analyze in a straightforward manner other types of discontinuities.

Acknowledgment

The authors wish to thank the reviewers for their helpful comments and suggestions.

References

[1] N. G. Alexopoulos, "Integrated circuit structures on anisotropic substrates," *IEEE Trans. Microwave Theory Tech.*, vol. MTT-11, pp. 847–881, Oct. 1985.

[2] H-Y. Yang and N. G. Alexopoulos, "Uniaxial and biaxial substrate effects on finline characteristics," *IEEE Trans. Microwave Theory Tech.*, vol. MTT-35, pp. 24–29, Jan. 1987.

[3] H. El Hennamy and K. Schunemann, "Impedance transformation in fin lines," *Proc. Inst. Elec. Eng.*, pt H, vol. 29, pp. 342–350, Dec. 1982.

[4] A. S. Omar and K. Schunemann, "Effect of complex modes on finline discontinuities," *IEEE Trans. Microwave Theory Tech.*, vol. MTT-34, pp. 1508–1514, Dec. 1986.

[5] A. S. Omar and K. Schunemann, "Transmission matrix representation of finline step discontinuities," *IEEE Trans. Microwave Theory Tech.*, vol. MTT-33, pp. 765–770, Sept. 1985.

[6] M. Helard, J. Citerne, O. Picon, and V. F. Hanna, "Theoretical and experimental investigation of finline discontinuities," *IEEE Trans. Microwave Theory Tech.*, vol. MTT-33, pp. 994–1001, Oct. 1985.

[7] R. Sorrentino and T. Itoh, "Transverse resonance analysis of finline step discontinuities," *IEEE Trans. Microwave Theory Tech.*, vol. MTT-32, pp. 1632–1638, Dec. 1984

[8] R. H. Jansen, "Hybrid mode analysis of end effects of planar microwave and millimeter wave transmission line," *Proc. Inst. Elec. Eng.*, pt. H, vol. 128, pp. 77–86, 1981.

[9] N. H. L. Koster and R. H. Jansen, "The equivalent circuit of the asymmetrical series gap in microstrip and suspended-substrate line,"

IEEE Trans. Microwave Theory Tech., vol. MTT-30, pp. 1273–1279, Dec. 1986.

[10] R. H. Jansen and N. H. L. Koster, "A unified CAD basis for the frequency dependent characterization of strip, slot and coplanar MIC components," in *Proc. 11th Eur. Microwave Conf.*, 1981, pp. 682–687.

[11] R. H. Jansen and N. H. L. Koster, "Some new results on the equivalent circuit parameters of the inductive strip discontinuity in unilateral fin lines," *Arch. Elek. Übertragung.*, pp. 497–499, 1981.

[12] J. B. Knorr, "Equivalent reactance of a shorting septum in a finline: Theory and experiment," *IEEE Trans. Microwave Theory Tech.*, vol. MTT-29, pp. 1196–1202, Nov. 1981.

[13] R. H. Jansen, "The spectral domain approach for microwave integrated circuits," *IEEE Trans. Microwave Theory Tech.*, vol. MTT-33, pp. 1043–1056, Oct. 1985.

[14] J. B. Knorr and J. C. Deal, "Scattering coefficients of an inductive strip in a finline: Theory and experiment," *IEEE Trans. Microwave Theory Tech.*, vol. MTT-33, pp. 1011–1017, Oct. 1985.

[15] N. H. L. Koster and R. H. Jansen, "The microstrip step discontinuity: A revised description," *IEEE Trans. Microwave Theory Tech.*, vol. MTT-34, pp. 213–223, Feb. 1986.

[16] H-Y. Yang, "Dispersive properties of finline and finline step discontinuities on anisotropic substrates for millimeter wave applications," Master's thesis U.C.L.A., Dec. 1985.

[17] R. Mittra and S. W. Lee, *Analytical Technique in the Theory of Guided Waves*. New York: Macmillan 1971.

[18] S. W. Lee, W. R. Jones, and J. J. Campbell, "Convergence of numerical solutions of iris-type discontinuity problems," *IEEE Trans. Microwave Theory Tech.*, vol. MTT-19, pp. 528–536, June 1971.

[19] H. Hofmann, "Dispersion of planar waveguide for millimeter wave application," *Arch. Elek. Übertragung.*, vol. 31, pp. 40–44, Jan. 1977.

[20] M. Olyphant, Jr., "Measuring anisotropy in microwave substrates," in *IEEE MTT-S 1979 Int. Microwave Symp. Dig.*, April 30–May 2, 1979, pp. 91–94.

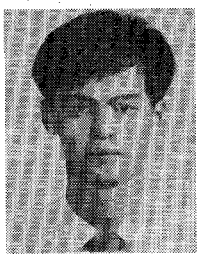

Hung-Yu Yang (S'87) was born in Taipei, Taiwan, on October 25, 1960. He received the B.S. degree in electrical engineering from National Taiwan University in 1982 and the M.S. degree in electrical engineering from the University of California at Los Angeles in 1985.

During 1982–1984, he served in the R.O.C. Navy as an electronics officer. He is currently working towards the Ph.D. degree at the University of California at Los Angeles. His research interests are in printed-circuit antennas and the modeling of microwave and millimeter-wave devices.

✠

Nicólaos G. Alexópoulos (S'68–M'69–SM'82–F'87) was born in Athens, Greece, in 1942. He graduated from the 8th Gymnasium of Athens, Greece, and subsequently obtained the B.S.E.E., M.S.E.E., and Ph.D. degrees from the University of Michigan, Ann Arbor, in 1964, 1967, and 1968, respectively.

He is currently a Professor in the Department of Electrical Engineering, University of California at Los Angeles, Associate Dean of the School of Engineering and Applied Science, and a Consultant with Northrop Corporation's Advanced Systems Division. His current research interests are in electromagnetic theory as it applies to the modeling of integrated-circuit components and printed circuit antennas for microwave and millimeter-wave applications, substrate materials and their effect on integrated-circuit structures and printed antennas, integrated-circuit antenna arrays, and antenna concealment studies. He is the Associate Editor of the IEEE TRANSACTIONS ON ANTENNAS AND PROPAGATION, *Electromagnetics Journal*, and *Alta Frequenza*.